PERFORMANCE ANALYSIS BETWEEN TWO SPARSITY-CONSTRAINED MRI

METHODS: HIGHLY CONSTRAINED BACKPROJECTION (HYPR) AND

COMPRESSED SENSING (CS) FOR DYNAMIC IMAGING

A Thesis

by

NIBAL ARZOUNI

Submitted to the Office of Graduate Studies of
Texas A&M University
in partial fulfillment of the requirements for the degree of

MASTER OF SCIENCE

August 2010

Major Subject: Electrical Engineering

PERFORMANCE ANALYSIS BETWEEN TWO SPARSITY-CONSTRAINED MRI

METHODS: HIGHLY CONSTRAINED BACKPROJECTION (HYPR) AND

COMPRESSED SENSING (CS) FOR DYNAMIC IMAGING

A Thesis

by

NIBAL ARZOUNI

Submitted to the Office of Graduate Studies of
Texas A&M University
in partial fulfillment of the requirements for the degree of

MASTER OF SCIENCE

Approved by:

Chair of Committee,	Jim Ji
Committee Members,	Jiang Hu
	Mary McDougall
	Raffaella Righetti
Head of Department,	Costas Georghiades

August 2010

Major Subject: Electrical Engineering

ABSTRACT

Performance Analysis Between Two Sparsity-Constrained MRI Methods: Highly

Constrained Backprojection (HYPR) and Compressed Sensing (CS) for Dynamic

Imaging. (August 2010)

Nibal Arzouni, B.S., University of Michigan Ann Arbor

Chair of Advisory Committee: Dr. Jim Ji

One of the most important challenges in dynamic magnetic resonance imaging (MRI)

is to achieve high spatial and temporal resolution when it is limited by system

performance. It is desirable to acquire data fast enough to capture the dynamics in the

image time series without losing high spatial resolution and signal to noise ratio. Many

techniques have been introduced in the recent decades to achieve this goal. Newly

developed algorithms like Highly Constrained Backprojection (HYPR) and Compressed

Sensing (CS) reconstruct images from highly undersampled data using constraints.

Using these algorithms, it is possible to achieve high temporal resolution in the dynamic

image time series with high spatial resolution and signal to noise ratio (SNR). In this

thesis we have analyzed the performance of HYPR to CS algorithm. In assessing the

reconstructed image quality, we considered computation time, spatial resolution, noise

amplification factors, and artifact power (AP) using the same number of views in both

algorithms, and that number is below the Nyquist requirement. In the simulations

performed, CS always provides higher spatial resolution than HYPR, but it is limited by

computation time in image reconstruction and SNR when compared to HYPR. HYPR

performs better than CS in terms of SNR and computation time when the images are sparse enough. However, HYPR suffers from streaking artifacts when it comes to less sparse image data.

TABLE OF CONTENTS

LIST OF TABLES

LIST OF FIGURES

CHAPTER I

INTRODUCTION

Many research projects have been going on in MRI to reduce acquisition time by reducing the amount of data necessary to produce MR images. However, the imaging speed is constrained by the quality of the reconstructed images. We need to increase the imaging speed without degrading the image quality. Researchers have introduced many techniques and algorithms to achieve this goal. Partial Parallel Imaging is one of those techniques that helped to reduce acquisition time using multiple receiver coils (1-3). Undersampling the K-space is used in many algorithms, but reducing the K-space size will result in many aliasing artifacts. Compressed Sensing and HYPR are both newly introduced algorithms to reconstruct images from highly undersampled data and mitigate undersampling artifacts (4-5). CS uses the implicit sparsity in MR images by transforming the images into a sparse domain using fixed mathematical approaches like the Discrete Cosine transform (DCT) and wavelet transform (6-7). CS suggests that if undersampling incoherent artifacts result in the transform sparse domain, the image can be reconstructed using an appropriate nonlinear method. On the other hand, HYPR was introduced in projection imaging permitting the use of decreased number of projections. HYPR is mainly used for sparse images like angiograms. It also reduces streak artifacts and enhances the SNR level in the reconstructed images.

_____

This thesis follows the style of *Magnetic Resonance in Medicine*.

While HYPR is mainly used with radial acquisition, CS can be used in many acquisition methods. Besides radial imaging, CS can also be used with Cartesian and spiral imaging. We have analyzed the performance of both algorithms using radial acquisition. Radial trajectories have many advantages over other acquisition methods. In radial trajectories, the spatial resolution of the reconstructed image doesn't depend on the number of acquired radial lines. The spatial resolution depends on the size of the imaging FOV. This means that if we sample the acquired MR signal longer, this will increase the k-space size and consequently it will increase the spatial resolution. Furthermore, radial trajectories are more robust to motion artifacts because it will result in more samples in the central k-space region.

In this study, we have analyzed and compared the performance of both algorithms in reconstructing MR images. In assessing the image quality, we studied the spatial resolution and SNR, and we also measured computation times and artifact powers. In the analysis, we considered different cases in which we used sparse images and less sparse images, and we also considered cases when the image series is static and dynamic. These two algorithms were selected for analysis because they are relatively new, and we need to know their performance when compared to each other. We need to know which algorithm can be a better fit to be used with certain types of image datasets. Both algorithms are affected by the sparsity of the reconstructed images, and both of them can be used with radial acquisition, so it is also important to know which is better when images of different sparsity levels are used.

CHAPTER II

THEORIES

A. Compressed Sensing (CS) in K-t Focuss

Compressed Sensing uses the sparsity which is implicit in the MR images. The non sparse images are transformed from the pixel domain to a sparse representation using a sparsifying transform which can be DCT, wavelet, or finite differences which is often used in CS for MRI (6-10). We have used Radial K-t Focuss which implements radial CS (11). In K-t Focuss, the radial measurements on the polar coordinate of k-t space is represented by v which can be written in matrix form as

$$v = MF_s RF_t \rho \qquad [1]$$

where ρ is the vector of pixel values of the unknown x-f spectrum of the dynamic images. F_t is the temporal Fourier transform to make the signal sparse. R is the radon transform, and F_s is the Fourier transform along the radial direction of the sinogram. M is the sampling operator along the radial trajectories in k-space.

ρ can be decomposed into a prediction term ρ_0 and a residual term $\Delta\rho$. The greatness of Focuss algorithm is that it can solve the l1 norm of the desired sparse solution $\Delta\rho$ by successively solving re-weighted l2 norm. As iterations go on, the solution $\Delta\rho$ becomes l1 minimized. The proof is provided in (12) .The radial k-t Focuss

solves iteratively the l2 optimization problem in equation [2] after using an implicit gridding method in each iteration that replaces projection and back projection.

$$\text{Min } \| q_l \|_2$$

$$\text{s.t } \| v - FW_l q_l - F\rho_0 \|_2 \leq \varepsilon \tag{2}$$

where W_l is a diagonal weighting matrix at the l-th Focuss iteration, and $\Delta\rho_{l+1} = W_l q_l$.

$$F = MSF_x F_y F_t \tag{3}$$

F_x and F_y are the Fourier transform along the x-direction and y-direction respectively. S is the resampling operator.

$$X_{rad} = SX_{cart} \tag{4}$$

X_{rad} and X_{cart} are the interpolated values on the radial trajectory and the estimated values on the Cartesian grid respectively. Radial k-t Focuss solves iteratively equation [2] until the solution $\Delta\rho_l$ converges. It is expected that CS will take time in image reconstruction since the reconstruction is an iterative nonlinear process in order to find the best solution that fits equation [2] among all possible solutions.

B. Highly Constrained Backprojection (HYPR)

Highly Constrained Backprojection is a dynamic projection imaging algorithm. In HYPR, a set of projections are taken for each time frame. These projections are way below Nyquist requirement. The projections at different time frames are interleaved so that there will not be any overlap in the projection data. In the reconstruction process, some or all of the sinograms are combined to form a composite image which contains some or all of the acquired data to constrain the backprojection process (13-14). The composite image is mainly formed by conventional filtered backprojection like inverse radon transform. The quality of the composite image determines the quality of the reconstructed time frames.

The different time frames are reconstructed by multiplying the composite image with the corresponding weighting image which is formed from the unfiltered backprojections of the time frame projections divided by the projections of the composite image taken at the same angles. Let C be the formed composite image, then the individual weighting image Wt is formed by

$$W_t = R^{-1}\left[\frac{P_t}{R(C)}\right] \qquad [5]$$

where P_t represents the projections taken at certain angles for time frame t, and $R(C)$ is the projections of the composite image taken at the same angles as the time frame t. R^{-1} is the unfiltered backprojection in order to form the weighting image (15).

Then, the reconstructed time frame $I_{recon,t}$ is formed by multiplying the weighting image

with the composite image.

$$I_{recon,t} = W_t C \qquad [6]$$

CHAPTER III

METHODS

In analyzing the performance of the two methods, we studied the quality of the reconstructed images according to spatial resolution, noise amplification factors, artifact power, and the required computation time. In the analysis of AP and spatial resolution, the added noise was removed.

A. Spatial Resolution

Spatial resolution is a very crucial factor in producing images especially from undersampled data. In this study, we analyzed the two algorithms with the goal to determine which has the best spatial resolution. We want to know which algorithm can detect the smallest object and result in less edge blurring. It is not very clear how to characterize the spatial resolution by a single parameter or number. The PSF contains information about the spatial resolution. A PSF of an impulse in all directions will produce perfect reconstruction and very high spatial resolution, but it is often very difficult to measure the PSF. We used the modulation transfer function to give a quantitative measure of the spatial resolution by calculating the edge spread function ESF and the line spread function LSF from the image domain. The ESF is easy to calculate in the image, and it shows how the edges are blurred within the image. The LSF is just the first derivative of the ESF. The narrower the LSF the better since it will be closer to an impulse. The MTF is calculated by taking the one dimensional Fourier transform of the LSF. It is expected that the edges in the same image are blurred in the

same way, so the MTF in one direction will correspond to the MTF for the whole system producing the image (16-17).

Taking the number of pixels from 10% to 90% ESF will be a good measurable quantity to characterize the performance of the two algorithms with respect to spatial resolution. The number of pixels (X) in the 10% to 90% ESF rise determines the value of the limiting spatial frequency (LF) which is around 3% -10% MTF. The limiting spatial frequency is measured in line pair per pixel and it is inversely proportional to the number of pixels (X) found in the 10% to 90% ESF (17-18). The lower the number of pixels, the higher the limiting frequency is, and the system will have a better spatial resolution because it will pass higher frequencies. In approximating the MTF, we just took the main lobe of the LSF and zeroed all other values because we just care for the edge and how it is blurred.

$$LF \infty \frac{1}{X}(Lp/Pixel) \qquad [7]$$

B. Noise Magnitude Amplification Factor

Signal to noise ratio (SNR) calculation methods usually take a region for the signal and a region for the noise from the background of the reconstructed image. This technique doesn't separate the noise from artifacts involved in the image that will affect the SNR calculation. Noise magnitude amplification factor was used instead of SNR in order to separate the noise from artifacts. Noise can be estimated from variations over different simulations. More than one simulation were performed to acquire data for each

reconstructed time frame after normalizing by the total energy of the original and reconstructed frames. Since we know the statistics of the noise and its power, we can calculate the noise magnitude amplification factors for each frame.

After acquiring the data from more than one simulation, the variance of all pixels in the reconstructed time frame was taken. The average noise magnitude amplification is calculated by taking the average standard deviation over all pixels within a time frame divided by the standard deviation of the added noise. The maximum noise magnitude amplification factor is also calculated. Thus, we have a measure of how noise is varying in the frames. In this way we can separate the noise from artifacts.

C. Artifact Power

Reducing artifacts in the reconstructed images is one of the main goals of using HYPR and CS. We analyzed the performance of both algorithms to determine which algorithm results in fewer artifacts. The artifact power is a good quantitative measure that we can rely on. The Artifact power (AP) can be calculated based on the square difference error between a reference image I_{ref} and the reconstructed image I_{recon}. The reference images are formed from fully sampled reconstructed images. The AP is defined as (3, 19-20).

$$AP = \frac{\sum_{(x,y)\in ROI} \| I_{ref}(x,y)| - | I_{recon}(x,y) \|^2}{\sum_{(x,y)\in ROI} | I_{ref}(x,y)|^2} \qquad [8]$$

ROI is the region of interest which can be a partial or the whole image. The denominator is a normalization factor which corresponds to the total energy of the reference image.

D. Computation Time

Time is always considered in MRI whether it is acquisition time or reconstruction time. The main point of undersampling the data is to reduce acquisition time because it is always desired to acquire and reconstruct images fast enough. In this study, the reconstruction time was recorded in each simulation using HYPR and CS. The reconstruction time for CS is relatively long when compared to HYPR. One way to mitigate this problem is by using parallel computing on multi core processors.

CHAPTER IV

SIMULATIONS AND RESULTS

We did many simulations using MATLAB (The Mathworks Inc. Natick, MA, USA) for both algorithms considering different cases. We used first a sparse phantom squares images, and a less sparse dynamic cardiac and dynamic contrast enhanced images. We did simulations considering both static and dynamic cases on an Intel™ Core™ 2 Duo T5800 2.00 GHz CPU. We have used K-t Focuss software for the compressed sensing using radial acquisition (11). We used different sparsity levels because the sparsity in the image domain affects both algorithms. HYPR works well when the images are sparse in the pixel domain. Also, CS uses a sparsifying transform to change the image from a pixel non sparse domain to a sparse domain, so non sparse images can be transformed into a sparse representation in order to find the minimized L1 norm.

A. Sparse Square Data Set

We constructed a set of seven 256x256 frames that change slightly over time to resemble the dynamic change of an image. The images are constructed from different size square features with a bright pixel and some dark pixels in two squares are added to see which method will detect small features. The images used are shown in Fig. 1. Additive white Gaussian noise is also added to the original images in order to compare the SNR levels in the reconstructed images. In this simulation, the number of projections used in HYPR is 30 projections which is way below Nyquist which requires 400

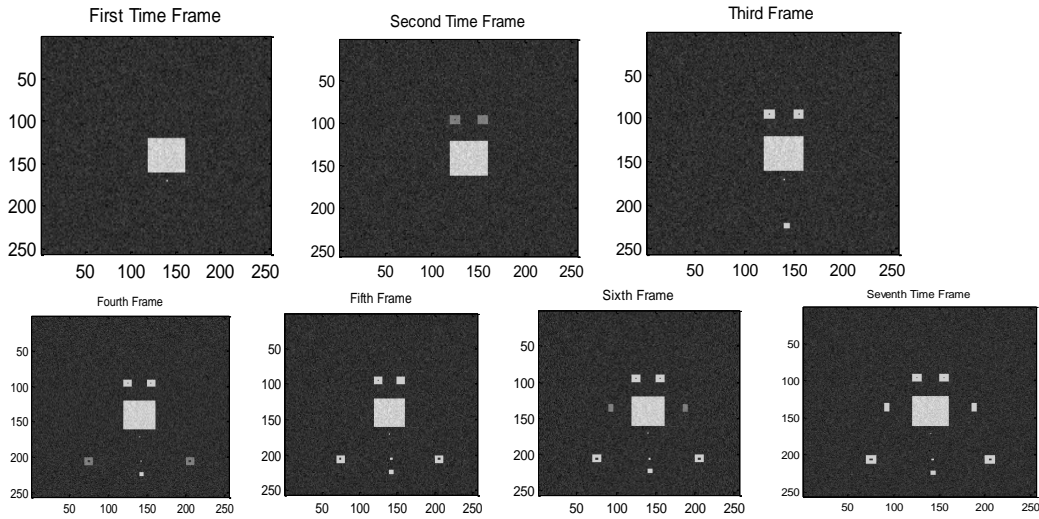Projections for a 256x256 image. We also took 30 radial projections per frame for CS reconstruction.

FIG. 1. The seven different sparse images used in the simulation

1- Static Sparse Features

In the first part of this simulation, we considered the static case where the sparse image is not changing over time. We just took the first frame repeated over time, and we used HYPR and CS to reconstruct the images in order to analyze the noise amplification, spatial resolution, and computation time. The reconstructed frames using both methods are shown in Fig. 2. In the HYPR reconstructed image, the bright pixel disappeared and

some artifacts are involved. All the reconstructed 7 frames in each case showed same level of SNR and spatial resolution.
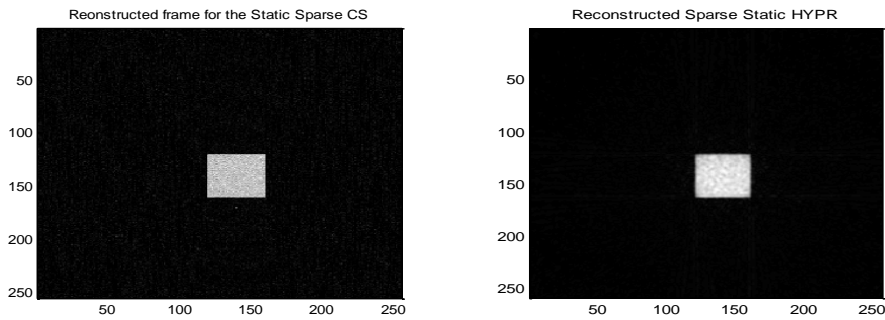

FIG. 2. The reconstructed images in the static sparse case

CS showed higher spatial resolution while HYPR showed higher SNR and less computation time but more artifacts are involved which can be discerned visually. The AP values calculated show that HYPR results in more artifacts. The AP values in the reconstructed images varied from 0.0091 to 0.0092 in CS and 0.0259 to 0.026 in HYPR. The approximate MTF of both HYPR and CS are shown in Fig. 3. The approximate MTF for CS is shown to pass all high frequencies. That is why it has a very high spatial resolution and it was able to detect the single bright pixel which disappeared in the HYPR reconstructed image.
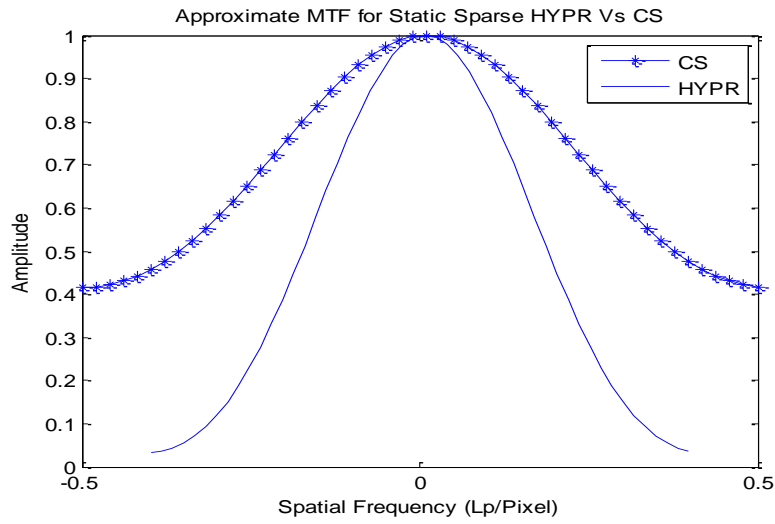
FIG. 3. The approximate MTFs of HYPR versus CS

Fig. 4 shows the ESF that is taken from the one of the reconstructed images.
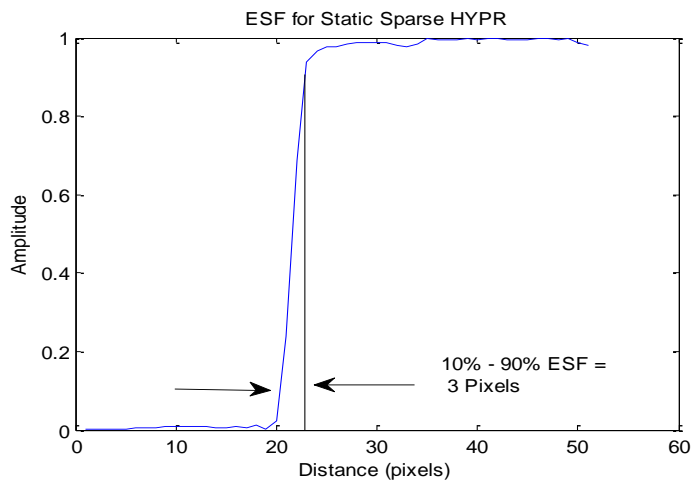

FIG. 4. The ESF of HYPR reconstructed image

The average noise magnitude amplification factor for both HYPR and CS showed that CS has higher noise amplification which implies that HYPR has better SNR. The average noise amplification is calculated for each time frame for the seven time frames using 10 different simulations. The spread plots of the average and maximum noise amplification with respect to each of the seven time frames are depicted in Fig. 5 and Fig. 6 respectively.
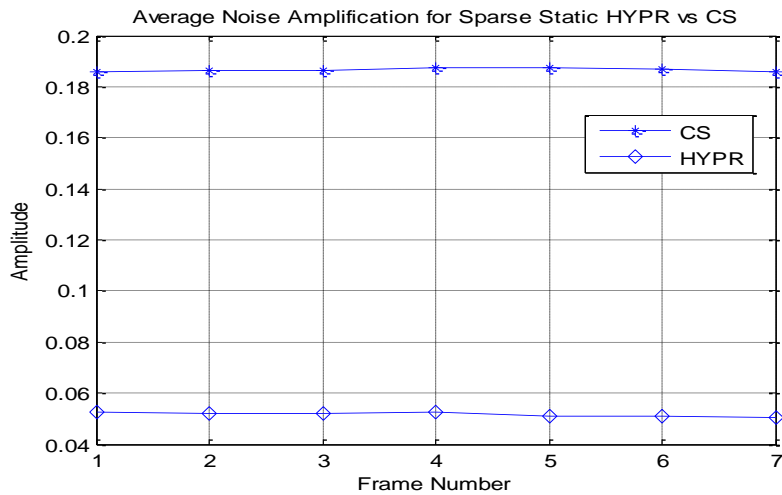

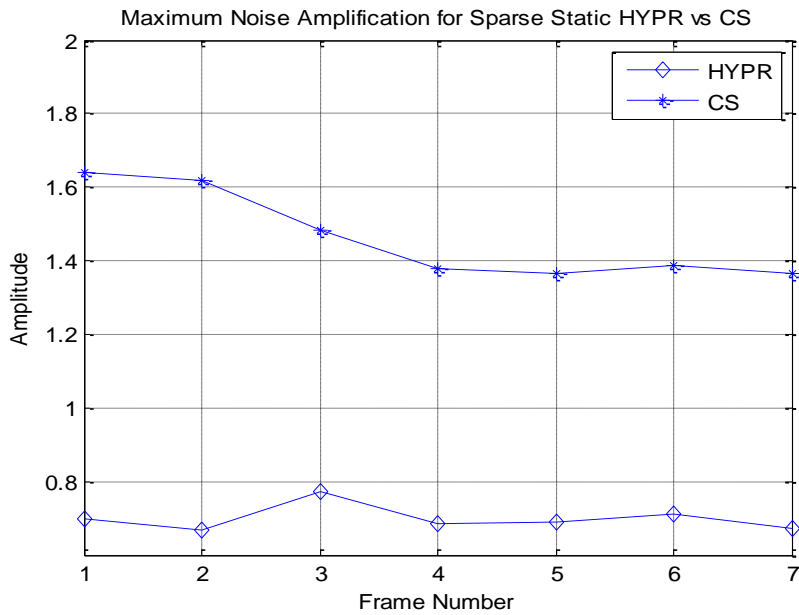FIG. 5. The average noise amplification for the sparse static HYPR vs CS

FIG. 6. The maximum noise amplification for sparse static HYPR vs CS

Table 1 shows the 10-90% ESF, computation time, and AP in the static sparse case for both HYPR and CS. The mean and standard deviation of the noise amplification for all 7 frames are taken.

Table 1

Results of the Static Sparse Case

	Average Noise Amplification	10 – 90% ESF (Pixels)	Computation Time (sec)	Artifact Power
HYPR	0.052± 0.0008	3	5.58	0.026
CS	0.187±0.1212	2	149.78	0.009

2- Dynamic Sparse Features

In the second part of this simulation, we considered the dynamic sparse case where we used the seven different frames that change gradually with time. Fig. 7 shows one of the reconstructed frames for HYPR and CS. Again, CS showed very high spatial resolution with sharp edges and fine details, and HYPR showed lower noise amplification and less computation time but more artifacts. In both CS and HYPR, dynamic imaging showed more artifacts than static imaging. The AP values in the CS case varied between 0.0081 and 0.0863 in the reconstructed images while the AP values varied between 0.0335 and 0.0863.
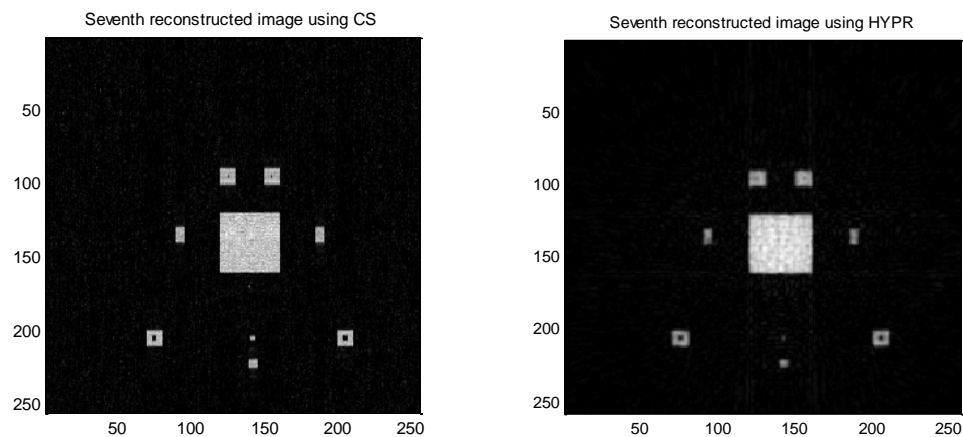

FIG. 7. HYPR reconstructed seventh frame versus CS

In the approximation of the MTF for HYPR and CS in the dynamic sparse case, we just took the ESF of one of the images since the spatial resolution is the same in all the reconstructed frames. The approximate MTF for both HYPR and CS looked the same thing as Fig. 3. This is expected since both static and dynamic showed same spatial resolution in both methods. The average noise amplification of HYPR versus CS in Fig.8 shows that HYPR has lower noise amplification which means it has higher SNR in the reconstructed images. Fig. 9 shows the maximum noise amplification for each time frame. Table 2 shows the different results for the sparse dynamic case.
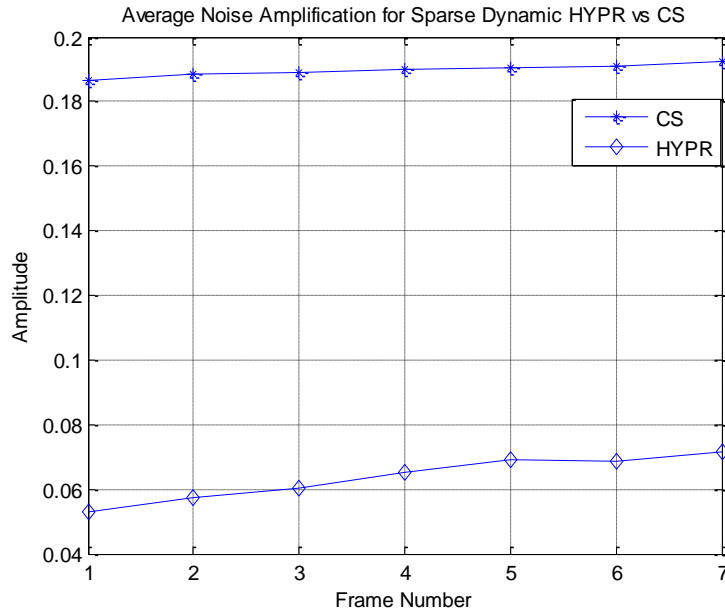

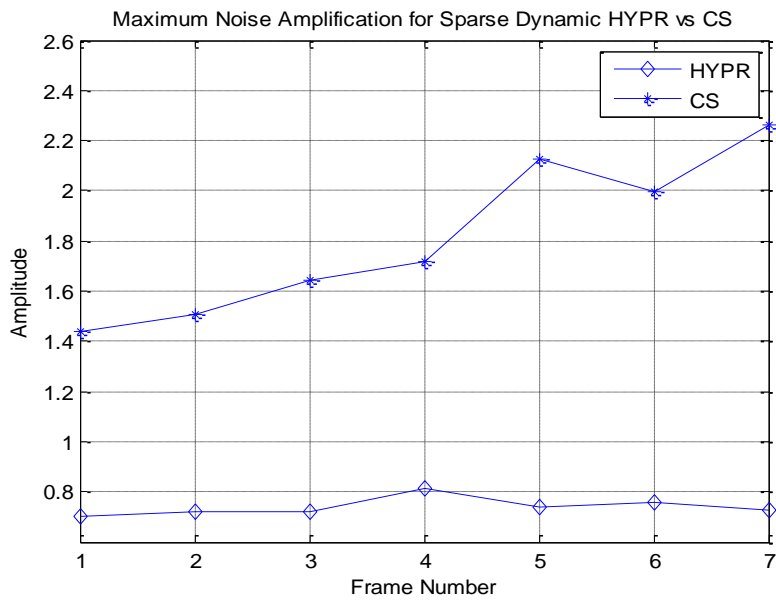FIG. 8. The average noise amplification for the sparse dynamic case

FIG. 9. The maximum noise amplification for the sparse dynamic case

Table 2

Results of the Dynamic Sparse Case

	Average Noise Amplification	**10 — 90% ESF (Pixels)**	**Computation Time (sec)**	**Artifact Power**
HYPR	0.064±0.007	3	6.74	0.033 − 0.122
CS	0.1897±0.002	2	187.42	0.008 − 0.086

B. Less Sparse Cardiac Data Set

HYPR is mainly used for sparse images like angiograms, but we tried to analyze the performance of HYPR relative to CS when the images are less sparse. In this simulation, we used dynamic cardiac images of 25 frames each of 256x256 size. We took the same number of views for both HYPR and CS which is 30 radial lines. First, we considered the static case when the images are not changing with time in that case we just took the first frame repeated over the 25 frames. Second, we analyzed the dynamic case where we used the changing 25 frames. Noise is added to the original images. Fig. 10 shows the first three of the original dynamic cardiac time frames.
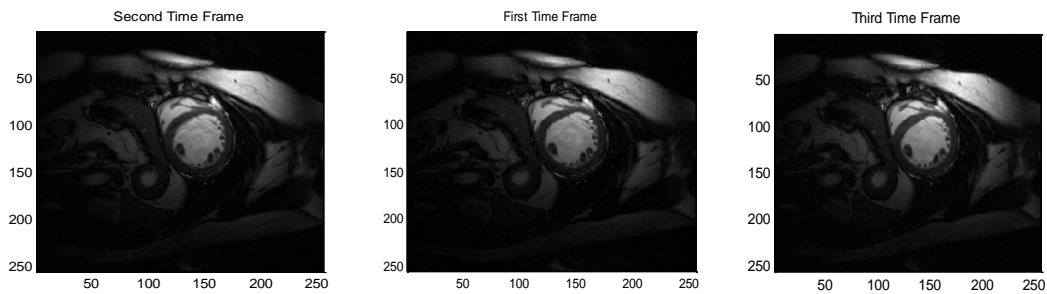

FIG. 10. The first three dynamic cardiac frames

1- Static Less Sparse Cardiac Features

In the static case, HYPR showed lower spatial resolution and more artifacts than CS which means that HYPR is not a good choice in reconstructing less sparse images. CS showed higher spatial resolution but more computation time. When it comes to SNR, HYPR showed low SNR compared to the results when we used HYPR in the reconstruction of sparse images. This can be shown in the spread plots of the average and maximum noise amplification factors with respect to time frames. Two of the reconstructed static images are shown in Fig. 11.
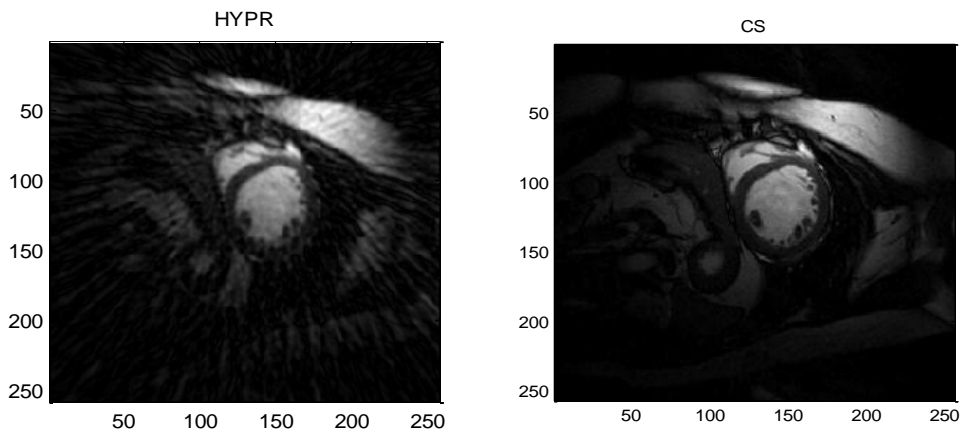

FIG. 11. The reconstructed images using HYPR and CS in the Static case

The approximate MTF of CS in Fig. 12 shows wider FWHM and higher limiting frequency than that of HYPR which is expected since the reconstructed images show higher spatial resolution in CS with finer details and sharper edges.
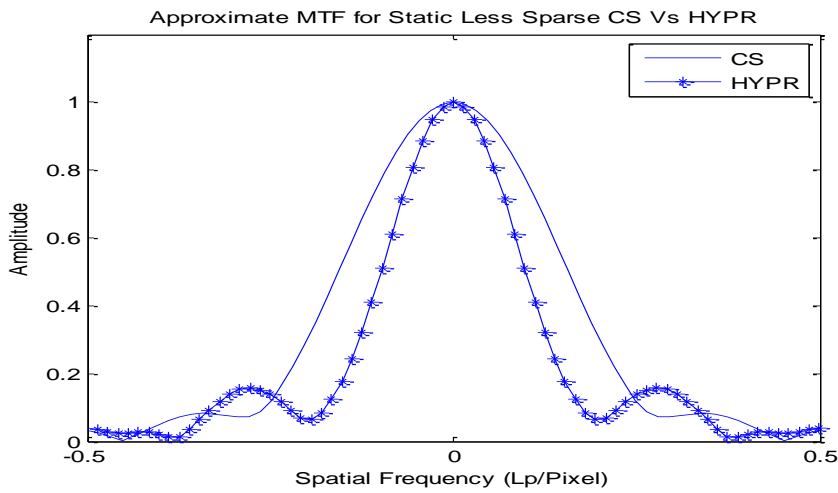

FIG. 12. The approximate MTFs in the static less sparse case

Fig. 13 and Fig. 14 show the average and the maximum noise amplification for HYPR versus CS. The results show that HYPR has higher average noise amplification than CS which means that HYPR is not a good fit for less sparse data sets. Table 3 shows the results of different parameters.
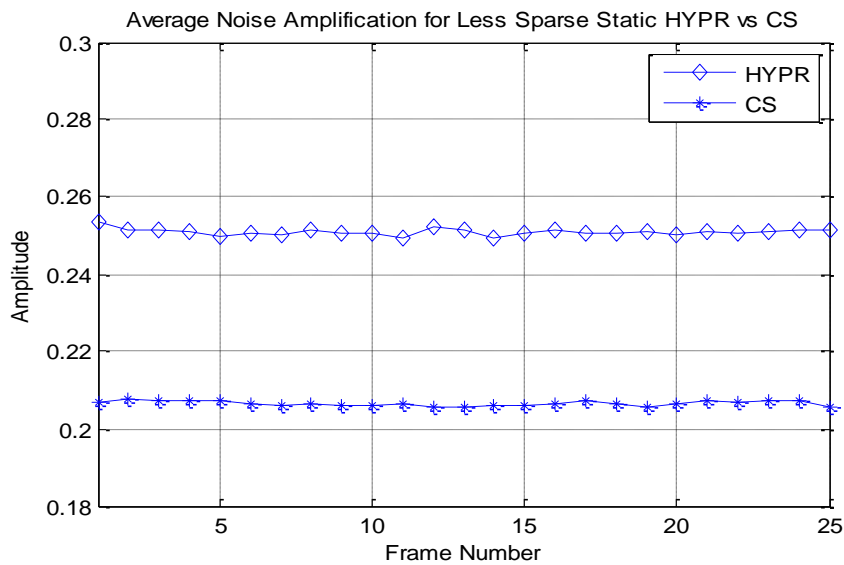
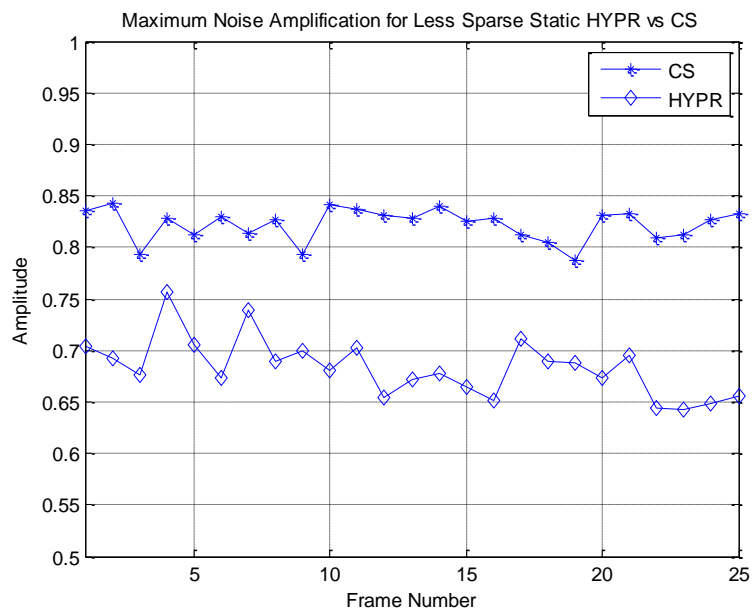FIG. 13. The average noise amplification for less sparse static case

FIG. 14. The maximum noise amplification for less sparse static case

Table 3

Results of the Static Less Sparse Cardiac Case

	Average Noise Amplification	10 — 90% ESF (Pixels)	Computation Time (sec)	Artifact Power
HYPR	0.251±0.0008	6	29.88	0.051 – 0.054
CS	0.206±0.0007	4	643.65	0.014 – 0.016

2- Dynamic Less Sparse Cardiac Features

In the second part of this simulation, we considered the dynamic case where we used the 25 changing cardiac images. Two of the reconstructed images of the same frame are shown in Fig. 15 for both methods. We can say that CS always provides higher spatial resolution compared to HYPR but the tradeoff is computation time. The approximate MTFs for both methods are shown in Fig. 16 which is very close to the static case. HYPR shows many streaking artifacts which suggest its weak performance in the reconstruction of less sparse data set. Table 4 summarizes the results.
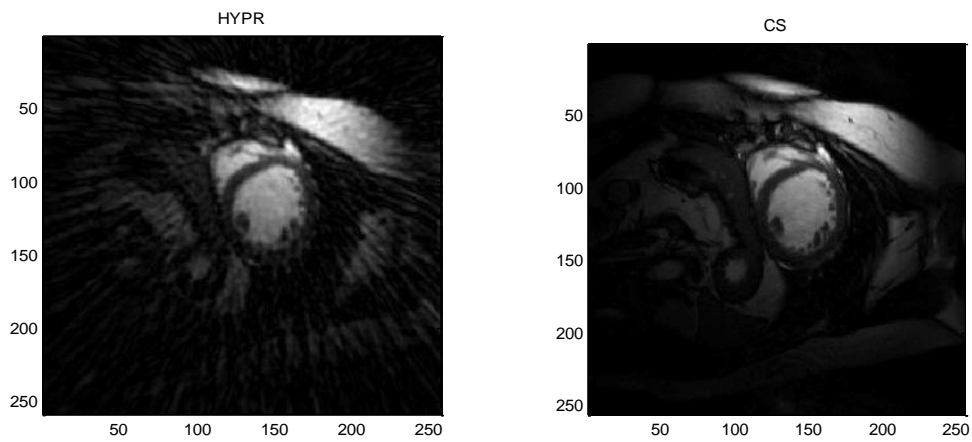
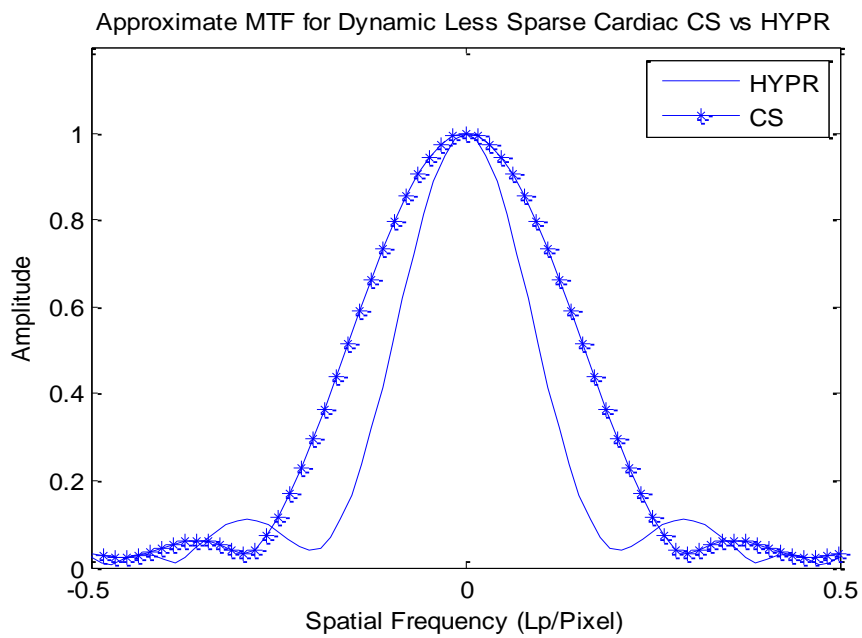FIG. 15. HYPR and CS reconstructed frames in dynamic less sparse case

FIG. 16. The approximate MTFs in the dynamic less sparse case

The average and maximum noise amplification plots are shown in Fig. 17 and Fig. 18 respectively.
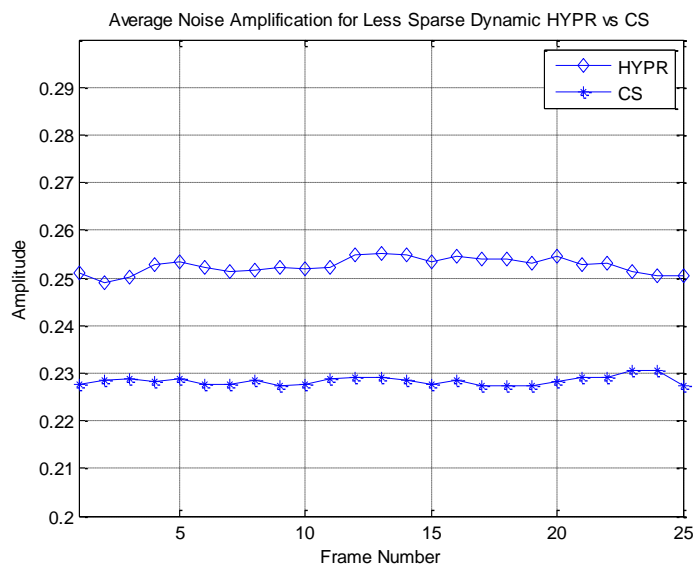

FIG. 17. The average noise amplification for less sparse dynamic case
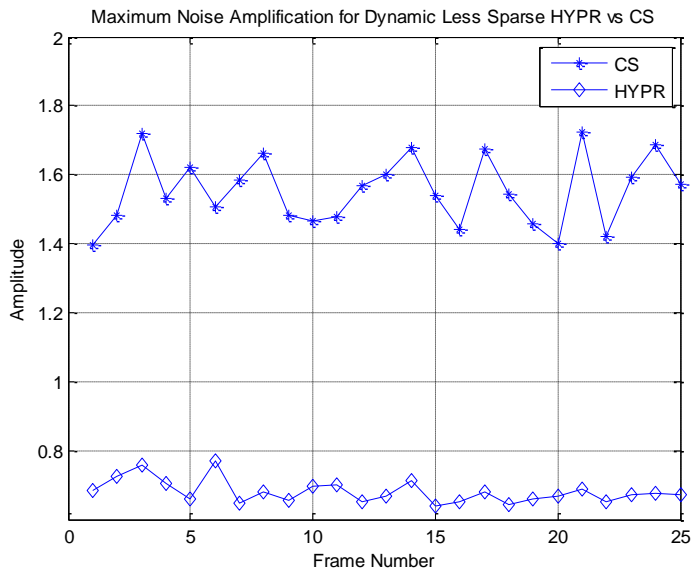
FIG. 18. The maximum noise amplification for less sparse dynamic case

Table 4

Results of the Dynamic Less Sparse Cardiac Case

	Average Noise Amplification	10 — 90% ESF (Pixels)	Computation Time (sec)	Artifact Power
HYPR	0.253±0.0016	6	29.12	0.042 – 0.188
CS	0.228±0.001	4	740.99	0.014 – 0.035

C. Less Sparse DCE Data Set

In this part, we used 22 frames of Dynamic Contrast Enhanced 128x128 images which are considered less sparse. Similarly, we analyzed the performance of both methods in the static and dynamic cases. We used the same number of views in both methods, and that number is 30 radial lines. Noise is also added to the original images where the first three frames are shown in Fig. 19.
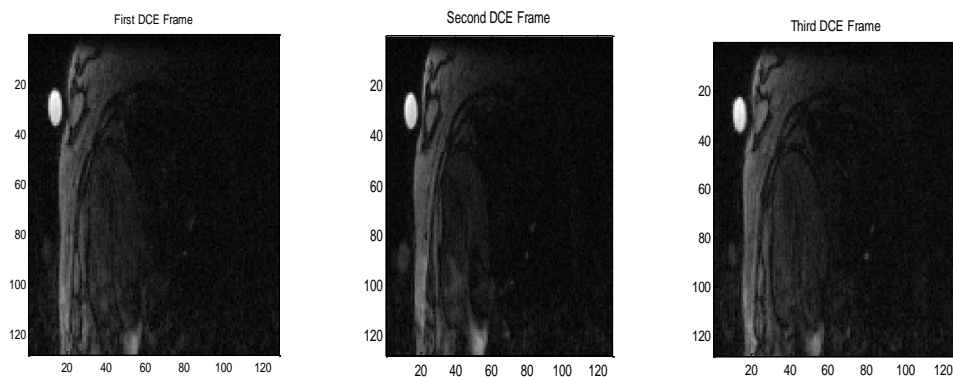

FIG. 19. The first three frames of the DCE data set

1- Static Less Sparse DCE Features

In the first part of the simulation, we considered the static case where we took the first frame over 22 time frames with no changes. The reconstructed images are shown in Fig. 20. The images show that CS is better in the reconstruction of less sparse images since HYPR results in many artifacts.
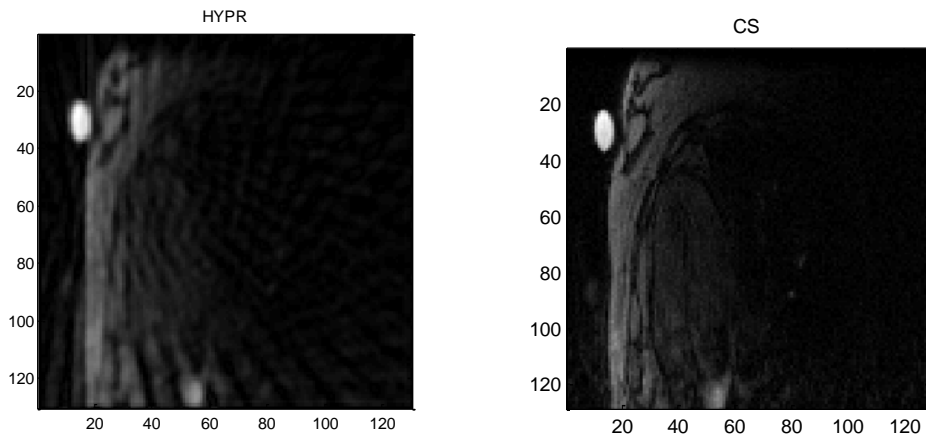

FIG. 20. HYPR and CS reconstructed frames in static less sparse DCE case

The approximate MTFs in Fig. 21 for both methods explain why CS has better spatial resolution and preserves the details which are somehow lost in HYPR reconstruction.
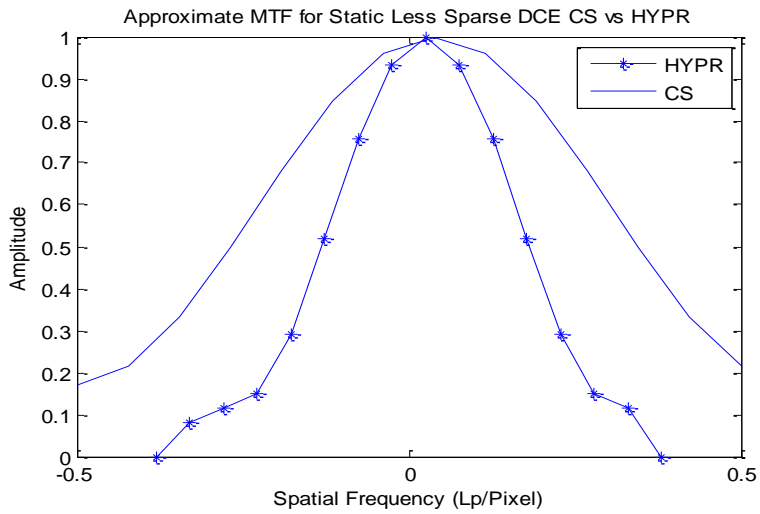
FIG. 21. Approximate MTFs in the Static Less Sparse DCE Case

The average and maximum noise magnitude amplification factor are shown in Fig. 22 and Fig. 23 respectively. Table 5 summarizes the results. We can see that CS is providing higher spatial resolution, and HYPR suffers from more streaking artifacts. The noise amplification spread plots show that HYPR has better performance which will result in a better SNR.
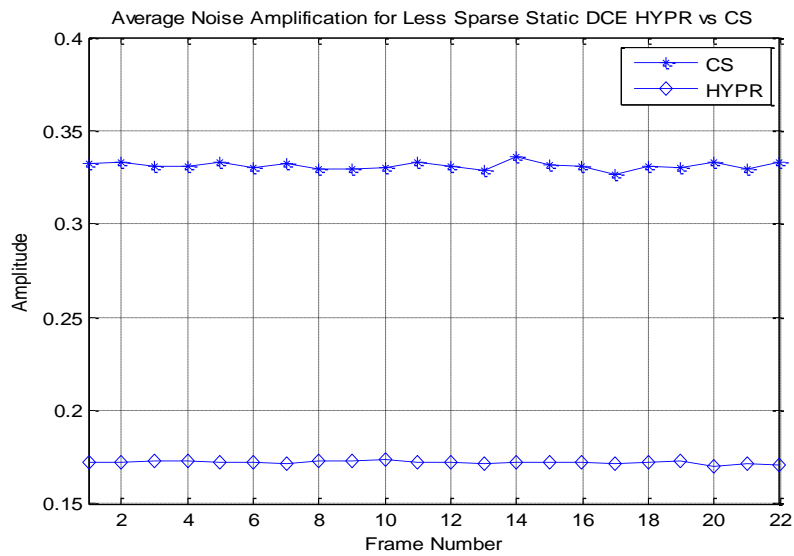
FIG. 22. The average noise amplification for the less sparse static DCE case

FIG. 23. The maximum noise amplification for the static less sparse DCE case

Table 5

Results of the Static Less Sparse DCE Case

	Average Noise Amplification	**10 — 90% ESF (Pixels)**	**Computation Time (sec)**	**Artifact Power**
HYPR	0.172±0.0008	3	5.49	0.096 – 0.11
CS	0.331±0.002	2	127.7	0.039 – 0.042

2- Dynamic Less Sparse DCE Features

In the second part, we considered the dynamic case where we took the changing 22 DCE frames. Results confirm that CS is much better than HYPR when we use less sparse datasets. Two of the reconstructed images from the two methods are shown in Fig. 24.
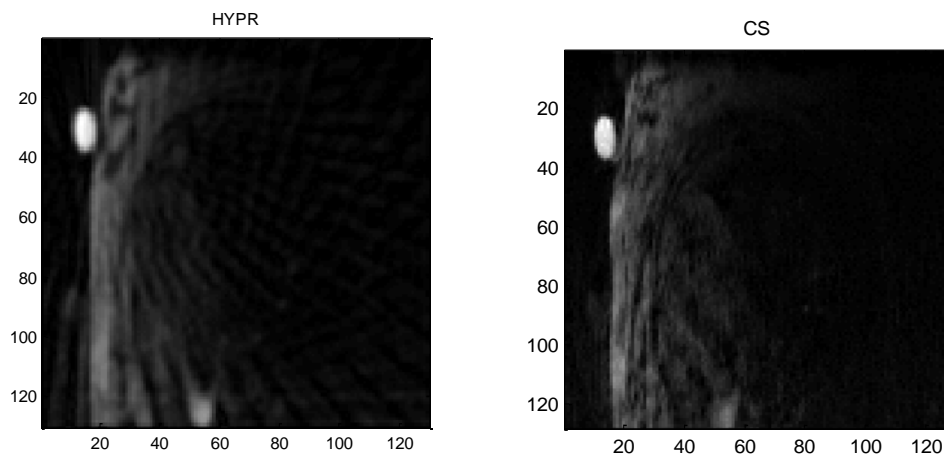
FIG. 24. HYPR and CS reconstructed frames in dynamic less sparse DCE case

The approximate MTFs of both HYPR and CS are shown in Fig. 25 which shows that the MTF of CS is much wider, and that is why CS has better spatial resolution.
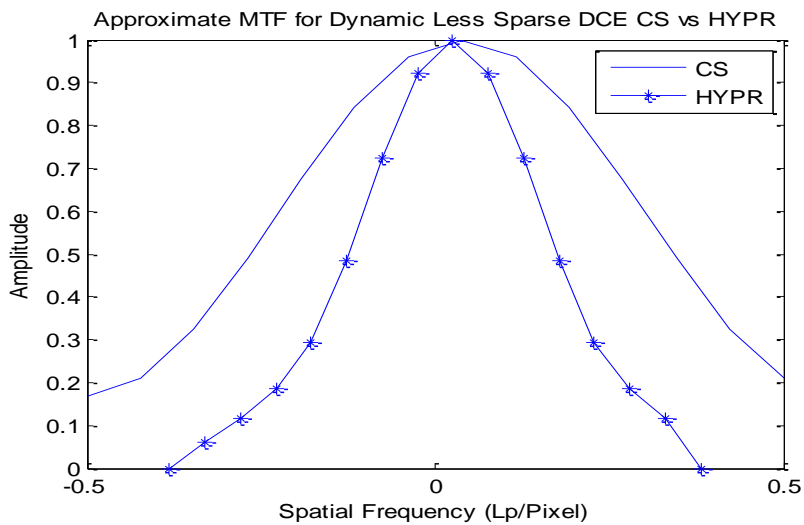

FIG. 25. The approximate MTFs in the dynamic less sparse DCE case

The average and maximum noise amplification versus the 22 time frames are depicted in Fig. 26 and Fig. 27 respectively. Table 6 summarizes the results.

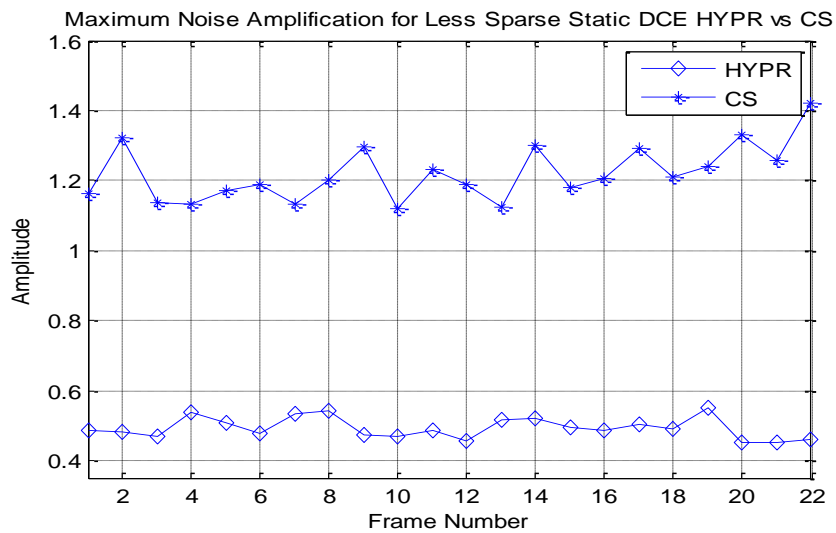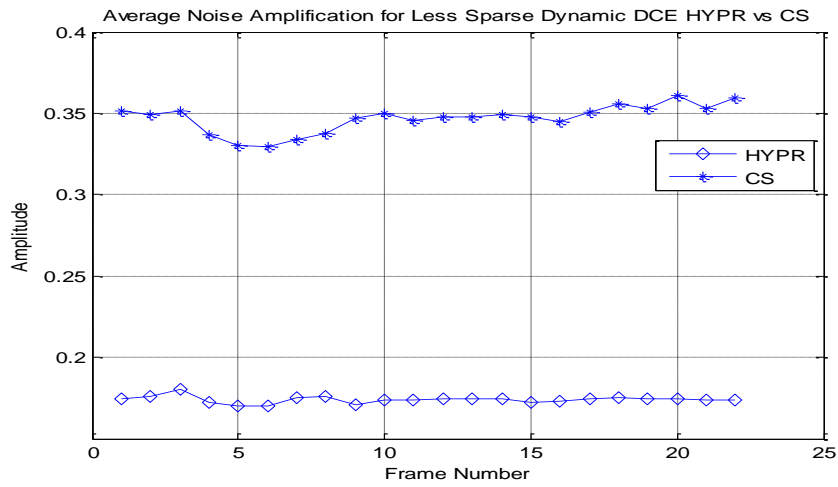FIG. 26. The average noise amplification for the dynamic less sparse DCE case
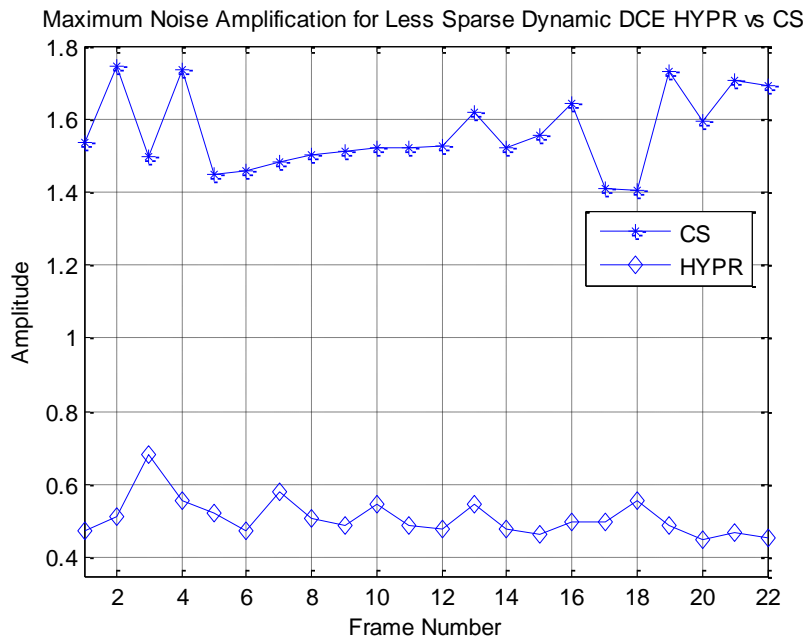
FIG. 27. The maximum noise amplification for the dynamic less sparse DCE case

Table 6

Results of the Dynamic Less Sparse DCE Case

	Average Noise Amplification	10 — 90% ESF (Pixels)	Computation Time (sec)	Artifact Power
HYPR	0.174±0.0021	3	9.24	0.082 – 0.138
CS	0.347±0.0085	2	122.55	0.043 – 0.077

CHAPTER V

CONCLUSION

In this study, we concluded that HYPR can be better than CS when sparse images are used since it shows less noise amplification, SNR enhancement, and smaller computation time. On the other hand, CS always provides very high spatial resolution where the reconstructed images preserve sharp edges and fine details. In the case of less sparse data sets, HYPR performance is very weak since it suffers from many streaking artifacts. In comparing the static and dynamic cases for both methods, we found that the spatial resolution is the same since the number of projections doesn't change the spatial resolution, but there are more artifacts involved in the dynamic case. In HYPR image reconstruction, dynamic imaging suffers from more artifacts than the static case because the composite image contains information from many different time frames. The study shows that HYPR works very well when the images are sparse, and HYPR is mainly used to image angiograms which are sparse in the pixel domain. The performance of HYPR is very weak and suffers from streaking artifacts when the images used are less sparse. HYPR is mainly used with radial acquisition which is still in use. One way to improve and optimize the performance of HYPR is if we can find a way to sparsify the time frames before applying HYPR. That will improve the performance of HYPR. CS works very well and produces images with high quality, but the only disadvantage is computation time which can be mitigated by using parallel computing on multi core processors. This study is mainly focused to present a good idea how the performance of the two algorithms will be in different cases, so it is an attempt to help in deciding which

method can be a better fit to use when thinking about different data sets. Table 7 below summarizes the results of this study where (>>>) means highly greater than and (~>) means slightly greater than.

Table 7

Summary of the Results in Different Cases (C for CS and H for HYPR)

	Noise Amplification	Spatial Resolution	Computation Time	Artifacts
Static Sparse	C > H	C > H	C >> H	H > C
Dynamic Sparse	C > H	C > H	C >> H	H > C
Static Less Sparse	H ~> C	C > H	C >>> H	H >> C
Dyn. Less Sparse	H ~> C	C > H	C >>> H	H >> C

REFERENCES

1.   Pruessmann K, Weiger M, Scheidegger M, Boesiger P. SENSE: sensitivity encoding for fast MRI. Magnetic Resonance in Medicine 1999;42(5):952-962.

2.   Sodickson D. Simultaneous acquisition of spatial harmonics (SMASH): Ultra-fast imaging with radiofrequency coil arrays. Google Patents; 1999.

3.   Ji J, Son J, Rane S. PULSAR: A Matlab toolbox for parallel magnetic resonance imaging using array coils and multiple channel receivers. Concepts in Magnetic Resonance Part B Magnetic Resonance Engineering 2007;31(1):24.

4.   Candes E, Romberg J, Tao T. Robust uncertainty principles: Exact signal reconstruction from highly incomplete frequency information. IEEE Transactions on Information Theory 2006;52(2):489-509.

5.   Candès E, Romberg J, Tao T. Stable signal recovery from incomplete and inaccurate measurements. Communications on Pure and Applied Mathematics 2006;59(8):1207.

6.   Donoho D. Compressed sensing. IEEE Transactions on Information Theory 2006;52(4):1289-1306.

7.   Gamper U, Boesiger P, Kozerke S. Compressed sensing in dynamic MRI. Magnetic Resonance in Medicine 2008;59(2):365-373.

8.   Lustig M, Donoho D, Pauly J. Sparse MRI: The application of compressed sensing for rapid MR imaging. Magnetic Resonance in Medicine 2007;58(6):1182-1195.

9. Lustig M, Donoho D, Santos J, Pauly J. Compressed sensing MRI. IEEE Signal Processing Magazine 2008;25(2):72-82.

10. Baraniuk R. Compressive sensing. Lecture notes in IEEE Signal Processing magazine 2007;24(4):118-120.

11. Jung H, Park J, Yoo J, Ye J. Radial kt FOCUSS for high-resolution cardiac cine MRI. Magnetic Resonance in Medicine 2009;63(1):68-78.

12. Jung H, Ye J, Kim E. Improved k--t BLAST and k--t SENSE using FOCUSS. Physics in Medicine and Biology 2007;52:3201-3226.

13. Mistretta C. Undersampled radial MR acquisition and highly constrained back projection (HYPR) reconstruction: Potential medical imaging applications in the post-Nyquist era. Journal of Magnetic Resonance Imaging 2009;29(3):501-516.

14. Mistretta C, Wieben O, Velikina J, Block W, Perry J, Wu Y, Johnson K. Highly constrained backprojection for time-resolved MRI. Magnetic resonance in medicine: Official journal of the Society of Magnetic Resonance in Medicine/Society of Magnetic Resonance in Medicine 2006;55(1):30.

15. O'Halloran R, Wen Z, Holmes J, Fain S. Iterative projection reconstruction of time-resolved images using highly-constrained back-projection (HYPR). Magnetic Resonance in Medicine 2008;59(1):132-139.

16. Webb A, Kagadis G. Introduction to biomedical imaging. Medical Physics 2003;30:2267.

17. Smith S. The scientist and engineer's guide to digital signal processing. Mustang, OK: Tate Publishing; 1997.

18. Bushberg J, Seibert J, Leidholdt Jr E, Boone J, Goldschmidt Jr E. The essential physics of medical imaging. Medical Physics 2003;30:1936.

19. Ji J, Son J, McDougall M, Wright S. Highly accelerated parallel imaging methods for localized massive array coils: comparison using 64-channel phased-array data. 2006. p 734-737.

20. McGibney G, Smith M, Nichols S, Crawley A. Quantitative evaluation of several partial Fourier reconstruction algorithms used in MRI. Magnetic Resonance in Medicine 2005;30(1):51-59.

VITA

Nibal Arzouni received his B.S. in electrical engineering and a minor in mathematics from the University of Michigan Ann Arbor summa cum laude in April 2008. He obtained his M.S. in electrical engineering from Texas A&M University in August 2010 where he had received a Graduate Merit Fellowship. He is planning to continue his Ph.D. degree at the University of Michigan Ann Arbor where he has also received a Rackham Graduate Merit Fellowship.

Address for correspondence:

Nibal Arzouni
Department of Electrical Engineering
Texas A&M University
214 Zachry Engineering Center
TAMU 3128
College Station, TX 77843